J. Fluid Mech. (1992), *vol.* 238, *pp.* 97–117
Printed in Great Britain

Interfacial waves in core–annular flow

By R. MIESEN, G. BEIJNON, P. E. M. DUIJVESTIJN, R. V. A. OLIEMANS AND T. VERHEGGEN

Koninklijke/Shell-Laboratorium, Amsterdam (Shell Research B.V.), Badhuisweg 3, 1031 CM Amsterdam, The Netherlands

(Received 13 February 1991 and in revised form 15 October 1991)

In this paper we present experiments and an analysis of interfacial waves in core–annular flow; these waves are important for the flow to be stable. The observed wave velocity is about equal to the speed of the fluids near the interface, and the wavelength is 1–10 times the thickness of the annulus. These results are predicted by our analysis, which is valid provided the Reynolds number of the fluid in the annulus, and the ratio of the viscosities of the fluids in the core and the annulus, are large. The theory gives the growth rate of a wave as a function of this ratio, the Reynolds number, the surface tension and the wavenumber. For parameter values of interest, the growth rate is positive for a range wavenumbers which we compare with the experiments. Qualitative agreement between theory and experiment is excellent; quantitative comparison reveals discrepancies for which a possible explanation is the neglect of nonlinear terms.

1. Introduction

For the transportation of very viscous crude oil, core–annular flow (CAF) can be an attractive alternative to heating or diluting the oil (see, for example, Wu *et al.* 1986). In lubricating CAF, the core (for example oil) is surrounded by a less viscous annulus (for example water). The fluid in the annulus reduces the pressure drop over the pipeline to the same order of magnitude as when only the less viscous fluid is present. Owing to the complicated hydrodynamics of CAF, the buoyancy on the core can be counterbalanced by pressure and viscous forces, resulting in a stable flow. It has been shown (Ooms *et al.* 1984; Oliemans & Ooms 1986) that waves on the oil/water interface play a crucial role in that balance. This leads to the paradox that the stability of CAF depends on the instability of the oil/water interface. The growth rate of interfacial waves is exponential in time according to linear theory. Of course, once the wave amplitude becomes finite, nonlinear effects will become important. These effects can saturate the linear growth (see, for example, Papageorgiou, Maldarelli & Rumschitzki 1990), resulting in waves with finite amplitudes and stable CAF, as observed in experiments (figure 1) with viscosity ratios ranging from 500 to more 10^5.

In this paper we present a linear analysis of the interfacial stability of oil/water CAF, together with experiments to study the waves at the interface of oil and water. The experiments were performed in two test loops, described in §2. Wavelengths and the average water layer thickness were measured. Characteristic values of the physical parameters involved are: pipe diameter ≈ 0.1 m, oil velocity ≈ 1 m/s, oil density ≈ 970 kg/m^3, oil viscosity ≈ 10 Pa s, water fraction in the pipe $\leqslant 0.15$, water layer thickness $d \approx 0.5$–5 mm. The Reynolds number for the water layer then is $R = O(10^3)$, the ratio of the viscosity of oil and water is $m = O(10^4)$, and the ratio of

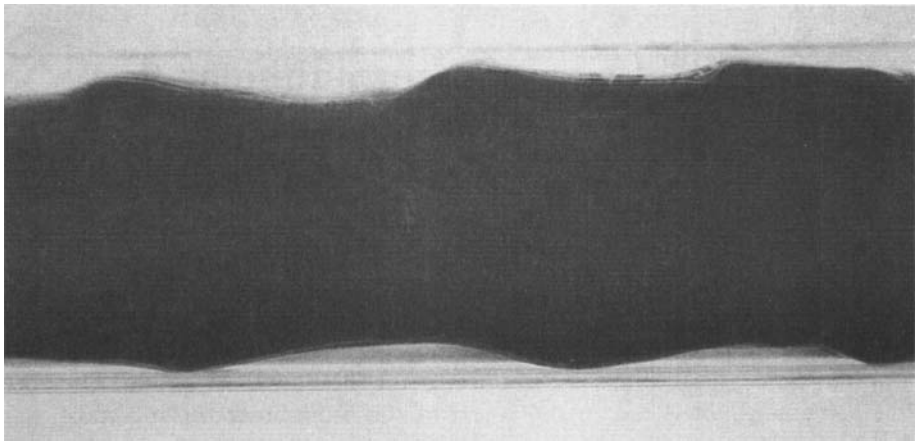

FIGURE 1. Waves observed in oil/water core–annular flow in a 2 in. pipe (flow direction from right to left). The superficial oil velocity was 0.5 m/s, and the oil viscosity was 3.5 Pa s. For this experiment a water fraction of 0.2 was used.

the radius of the oil core and the water layer thickness is $n > 10$. Observed wavelengths λ were typically of the order of ten times the water layer thickness, that is of the order of the pipe radius, giving a dimensionless wavenumber $\alpha := (2\pi/\lambda)\, d$ of the order of one.

The difference in viscosity between the fluids is an important cause of instability (Yih 1967). As already mentioned, for crude oil and water the viscosity ratio can be very large, more than 10^5 for very viscous crude oil. The instability exists irrespective of the magnitude of the Reynolds number, and is therefore not the high-Reynolds-number instability observed in Poiseuille flow, but rather the viscous analogue of the Kelvin–Helmholtz instability. There is an extensive literature on the analysis of the instability of a liquid/liquid interface due to a viscosity difference, which can be divided roughly into five groups: papers studying by asymptotic means the stability of the interface with respect to perturbations that are 'long', 'short' and 'intermediate' in length, papers studying the stability numerically, and papers dealing with nonlinear theory. We will review each group and discuss their relevance to our experiments.

Yih (1967) considered two-dimensional plane Couette–Poiseuille flow of two superposed layers of fluids of different viscosities between two horizontal plates. His analysis applies to the stability of the interface with respect to 'long' waves, that is waves that are much longer than Max $(2\pi d_i R_i)$, where d_i and R_i are thickness of the layer and the Reynolds number of fluid i $(i = 1, 2)$, respectively. Under this condition his analysis is valid for all ratios of the viscosities of the two fluids and for all ratios of the thicknesses of the layers. Flows with a thin layer of less viscous fluids at a wall, corresponding the most closely to what we have called lubricating flow, are found to be stable to these long-wavelength perturbations. In agreement with this, the waves we observe do not satisfy the long-wave conditions mentioned above. They are therefore not likely to be explained by a long-wavelength instability. Hooper (1985) studied linear stability of Couette flow for 'long' waves if one of the fluid layers is very thin compared to the other layer. She found that the flow is always unstable if the fluid in the thin layer is the more viscous one. Than, Rosso & Joseph (1987) extended the analysis of Yih (1967) by considering plane Poiseuille flow of two fluids in three layers, again restricting perturbations to long waves. For these

perturbations they showed that the interfaces for flow with the high-viscosity fluid centrally located (lubricating flow) are always stable, while interfaces for a flow with the less viscous fluid centrally located are unstable. With respect to long waves, Hickox (1971) considered the problem for a cylindrical geometry and axisymmetric undisturbed flow. However, he only evaluated his expressions for cases where the less viscous fluid is located centrally, and found that in that case the interface is never stable. Joseph, Renardy & Renardy (1984) studied numerically, and excluding gravity and surface tension, the configuration studied by Hickox (1971), but with the more viscous fluid located centrally and for viscosity ratios of $O(1)$. Like Yih (1967) for a two-dimensional geometry, they found that the interface for this flow is stable with respect to long waves if the annulus is thin. This is again consistent with the fact that we do not observe 'long' waves.

Hooper & Boyd (1983) studied the stability of the interface of two fluids of different viscosity in an infinite region, for two-dimensional Couette flow. They also considered the energy equation for this type of flow. If surface tension is neglected the interface is always unstable to waves of very small wavelengths. With respect to CAF this geometry seems to apply only if the waves are 'short', i.e. much shorter than the thickness of the thinner layer (the annulus). However, as we will see, these waves are stabilized by surface tension. Furthermore, Hooper & Boyd (1983) solved the stability problem exactly for unbounded Couette flow. The equation from which the growth rate follows is evaluated numerically. This equation is also studied in several asymptotic regimes, one of which (infinite viscosity ratio) yields the same result as the short-wavelength limit of the result of the analysis in this paper.

Renardy (1985) notes that the asymptotic analyses for 'long' waves (e.g. Yih 1967) and 'short' waves (Hooper & Boyd 1983) for Couette flow between two plates may miss unstable situations: waves with 'intermediate' wavelengths may have positive growth rates. She also notes, as Hooper & Boyd (1983) did for 'short' waves, that, for certain values of the parameters (e.g. viscosity ratio, surface tension, Reynolds number), the effects of an unstable density stratification (at the top of the cross-section of a pipe, for instance) can be compensated by viscosity stratification and surface tension, if the layer with the lower viscosity is thin enough. Hooper & Boyd (1987) present a two-dimensional analysis of the interfacial stability of Couette flow of two fluids of different viscosity, with respect to perturbations with 'intermediate' wavelengths. They show that the interface of a fluid that is bounded by a wall and an infinite fluid can be unstable to these perturbations if the bounded fluid is the less viscous one (lubricating flow). We shall return to their results later.

Yiantsios & Higgins (1988) studied numerically the interfacial stability of two fluids in plane two-dimensional Poiseuille flow, including density differences and interfacial tension, for a variety of physical parameters. Preziosi, Chen & Joseph (1989) studied numerically the stability of the interface in CAF in a cylinder geometry with the core fluid as the more viscous one, and they include surface tension and non-axisymmetric disturbances. The parameter values they use apply to experiments by Charles, Govier & Hodgson (1961), in particular the viscosity ratio of the two fluids, which is approximately 19. It is found that the axisymmetric disturbances are always the more unstable ones. Attention is paid to an instability of the interface and of the entire flow that cannot be studied in a plane geometry, and which is due to surface tension. As discussed in the introduction of the paper Papageorgiou *et al.* (1990) this instability can easily be understood in energetic terms: for axisymmetric disturbances with wavelengths larger than the circumference of the interface, the interfacial energy (area times interfacial tension)

decreases as the amplitude of the disturbance increases. Thus, while the axial component of the interfacial tension always acts to stabilize disturbances (with small wavelengths damped the most), the circumferential component can destabilize the interface. This capillary instability of the interface can be stabilized by the viscosity difference between the two fluids if the Reynolds number is large enough. In practice, this leads to a minimum velocity of the oil below which CAF is not stable.

Concerning the development of nonlinear theory for interfacial waves, Hooper & Grimshaw (1985), for Couette flow, and Shlang *et al.* (1985), for Poiseuille flow, extend the analysis of Yih (1967) for 'long' waves to include (weakly) nonlinear effects. They show that the evolution of the interface is governed by the Kuramoto–Sivashinsky equation, and that nonlinear effects, as well as surface tension, do indeed stabilize interface disturbances and can result in finite-amplitude steady states. On the other hand, quasi-periodic and chaotic solutions of this equation exist too. Hooper (1985) derives a weakly nonlinear evolution equation for interfacial waves if one of the fluid layers is very thin, but solutions of this equation are not given. In a recent study Papageorgiou *et al.* (1990) extended the weakly nonlinear theory by adopting an approach used by Frenkel *et al.* (1987) in their study of the nonlinear saturation of the capillary instability of CAF in the absence of viscosity differences. Papageorgiou *et al.* (1990) studied the stability of the interface of CAF in a cylindrical geometry in the limit of small film thickness including the dynamics of the core and surface tension. This leads to a modified Kuramoto–Sivashinsky equation having regular, nonlinear, travelling wave solutions for a large part of the parameter space. Their nonlinear expansion breaks down if the viscosity ratio of the fluids is larger than the ratio of the core radius and the thickness of the annulus.

The parameter values ($\alpha = O(1)$, $R \gg 1$) that apply to the experiments presented in this paper, and the geometry of a thin layer of less viscous fluid bounded by a wall and the interface with a very thick layer of more viscous fluid, seem to point to an interfacial instability as explained by Hooper & Boyd (1987) in a study of the 'intermediate' wavelength instability in a similar geometry. However, as Hooper & Boyd already note, and as is evident from the equations with which they start their analysis, their asymptotic results, obtained for $(\alpha R)^{\frac{1}{3}} \gg 1$ and $\alpha/(\alpha R)^{\frac{1}{3}} \ll 1$, are valid only for moderate m (the ratio of the viscosities of oil and water). We checked this numerically and found that, for the parameters of interest with respect to the experiments presented here, the analysis of Hooper & Boyd (1987) is valid if m is smaller than, 3, say, with $\alpha R > 10^3$. Hooper & Boyd (1987) also gave a dispersion relation that is valid for all parameters values. However, this equation is quite complicated, requires numerical solutions, and does not give us insight into how the growth rate depends on the parameters in the model. Therefore we present here (§3) an asymptotic analysis of the stability of the interface of planar Couette flow, taking into account that $m \gg 1$. A similar analysis was done (independently) by Hu, Lundgren & Joseph (1990), who address the stability of the interface in CAF with a very viscous core, for axisymmetric disturbances, and neglecting surface tension. The first case they consider is for interfacial waves with phase speeds that are clearly smaller than the speed of the oil core. Small growth rates are found for these modes. Their second case, for interfacial waves with phase speeds close to the speed of the oil core, is equivalent to the analysis presented here, if surface tension is neglected in our analysis, and using the fact that we consider a thin annulus. As a check on the accuracy of the asymptotic results, the linear stability problem is also solved numerically, using truncated expansions in terms of Chebyshev polynomials, and

solving the eigenvalue problem for the growth rate of the disturbances. Finally (§4), the results of the analysis and the experiments are compared.

2. Experiments

The experiments were carried out in a test loop, of 2 in. diameter, and 16 m long, and also in a second test loop, of 8 in. diameter, and 1000 m long. A diagram of these (similar) loops is given in figure 2. The oil is stored on top of a water layer in a tank. The temperature of the oil can be changed so that the viscosity of the oil can be varied. From the tank the oil is pumped to the inlet device, where the water layer is introduced around the oil core. Sometimes a solution of sodium silicate in water is added to the water (to a concentration of 0.2%) to make the pipe wall more hydrophilic and thus prevent fouling of the pipe wall by oil. The flow passes the test section in the CAF mode, a separator where most of the water is removed, and then returns to the tank. There, the oil and the remaining water will separate again as a result of their different densities. The 2 in. (8 in.) diameter test loop contains two (four) straight parts, each 6 m (250 m) long. The instrument section, provided with five ultrasonic transducers that measure the profile of the interface, was mounted 3 m (500 m) downstream of the inlet device. The transducers were distributed over half the pipe circumference at equal spacings of 45° in the same cross-sectional plane. In this paper only the data from the topmost transducer are used in comparisons with the theoretical predictions. The measuring technique is based upon ultrasonic reflection: a sound wave travelling through the water film is partially reflected at the oil/water interface. By recording the time between transmission and arrival of the reflected signal, and using the known speed of sound in water, the thickness of the water layer can be determined. The ultrasonic transducers used in the experiments operate both as transmitters and, a few microseconds later, as receivers. After each measurement (sample frequency 3052/s) the computer reads the counter, converts time into distance and stores the resulting value in its memory.

The resolution of the measuring system for determining the water layer thickness is 0.1 mm. Oil and gas bubbles and small particles in the water layer can cause early reflections, while on the other hand no echoes will be received from steeply sloping interfaces. Special algorithms for detecting these effects and restoring the signal were implemented. Accuracy in the measurement of the shape of the interface is mainly restricted by the fact that the ultrasonic beam is emitted from a transmitter which is a surface source with a diameter of 5 mm. For this reason, the lower limit for wavelengths that can be detected is 5 mm, where wavelength is defined as the distance between two successive wave tops. Accuracy of information about the exact shape of the surface will decrease as disturbances have smaller lengths. After a given data sampling period the data, containing values of the thickness of the water layer, are scanned for successive maximum values. The time between maxima is converted into distance using the speed of the oil core. This speed can be calculated from the amount of oil that is pumped into the pipe and the measured water hold-up. This is correct, as the velocity in the very viscous oil core is (almost) constant. Besides, the velocity of the disturbances on the interface was measured to be almost equal to the core velocity. Finally, the distances between the successive maxima give us the distribution of wavelengths that are present in the disturbance of the interface and which we will use to compare theoretical predictions with. The correctness and detail of the data were confirmed by bench-scale tests, using rigid wave profiles of known dimension and shape.

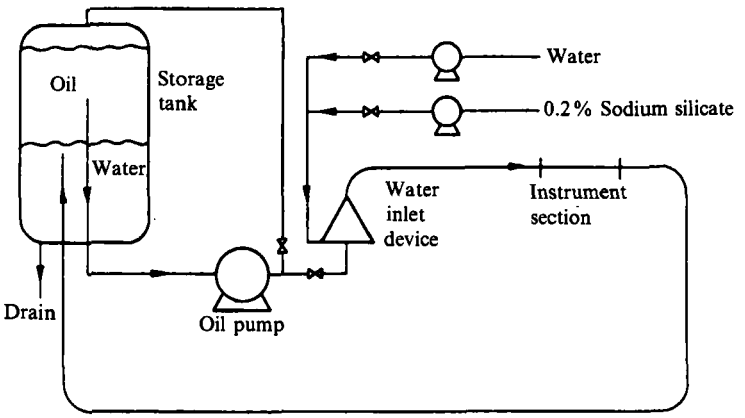

FIGURE 2. The core–annular flow test loop.

	2 in.	8 in.
Oil type	fuel	crude
Oil temperature (C°)	32–17	42–30
Oil viscosity (Pa s)	3.9–25	7–27
Oil density (kg/m^3)	957–971	978–992
Water temperature (°C)	10	25–20
Water viscosity (10^{-3} Pa s)	1.3	0.9–1.0
Water density (kg/m^3)	1000	998

TABLE 1. Experimental conditions

Experimental conditions are given in table 1. The superficial oil velocity (this is the velocity that the oil would have if no water were added) was varied between 0.5 and 2 m/s. For superficial oil velocities lower than 0.25 m/s (0.15 m/s) for the 2 in. (8 in.) pipe, the core tended to float against the upper part of the pipe, so that we did not observe the capillary, low-Reynolds-number, instability discussed by Preziosi *et al.* (1989). The input water fraction ranged between 0.04 and 0.14. A characteristic value for the oil/water interfacial tension is between 0.02 and 0.05 N/m.

The above figures give a variation between 3000 and 30000 for the ratio of the viscosities of oil and water. The ratio of the radius of the oil core and the thickness of the water layer was measured to vary between 10 and 50. The Reynolds number, based on the thickness of the water layer, the kinematic viscosity of water, and the velocity of the water at the interface had a minimum of, say, 250, and a maximum of about 10000.

The pressure gradient was typically twice the pressure gradient for the equivalent flow rate of only water. For the 2 in. pipe its value varied between 100 and 2000 Pa/m, and for the 8 in. pipeline between 25 and 250 Pa/m. The oil core is in general oval in shape and more or less concentrically located in the pipe. The minimum water layer thickness occurs at the sides of the pipe. The amplitudes of the waves on the interface are less than half the average water layer thickness. The speed of the waves was determined by cross-correlating the signals of two transducers mounted at the top of the pipe at an axial distance of 100 mm. It was found to be equal to the speed of the oil core, within the experimental error of about 10%. This is also the error in the measured wavelength. The dimensionless wavenumber

$\alpha(:= (2\pi/\lambda)d)$ of the interfacial waves (where λ is the wavelength and d is the thickness of the water layer) was between about 0.2 and 2 for most runs. The maximum of the wavelength distribution occurred at approximately 0.4. A more detailed account of the data on the observed wavelengths is given in §4, where a comparison with the predictions of the model that is presented in the next section is made. The water hold-up, that is the volume fraction of water present in the pipe, was found to be greater than the input water fraction by a factor of 1.0–1.3. This means that the average velocity of the water layer is smaller than the velocity of the core, but not by the factor of 2 that would be found for a linear velocity profile between a flat interface and the wall. This is due to the finite amplitudes of the waves, disturbing the basic flow, and probably an important cause of disagreement between theory and experiment.

3. Analysis

3.1. *The model*

As the basic flow we use two-fluid Poiseuille flow. The two fluids, separated by a cylindrical interface, are located concentrically (Oliemans 1986). This basic flow is a solution of the Navier–Stokes equations if gravity is neglected ('density-matched flow'). If the annulus is much thinner than the core, and the fluid in the core is much more viscous, the velocity of the fluid in the annulus varies linearly between the wall and the interface, while the velocity of the fluid in the core is constant. This can be shown as follows. The solution for the basic flow of the Navier–Stokes equations in a cylindrical geometry is given by equation (4.2) of Preziosi *et al.* (1989). The ratio of the inner radius of the pipe R_2 and the radius at which the interface of the two fluids is located R_1 is given by $a = R_2/R_1 = 1+n^{-1}$, where $n \gg 1$ is the dimensionless core radius R_1/d. The distance to the centre of the pipe divided by R_1 is r, and the ratio of the viscosity of the fluid in the core (oil) and the fluid in the annulus (water) is given by m (note that Preziosi *et al.* define m the other way round). If the velocity profile in the pipe is normalized with the centreline velocity it is found that the basic flow is given by

$$U(r) = \begin{cases} 1-r^2/[m(a^2-1)+1], & 0 \leqslant r \leqslant 1, \\ m(a^2-r^2)/[m(a^2-1)+1], & 1 \leqslant r \leqslant a. \end{cases} \tag{1}$$

If we define the distance to the interface as $z := r-1$, and use $a = 1+n^{-1}$, $m \gg n \gg 1$, it is found that

$$U(z) \approx 1-nz(1+\tfrac{1}{2}z)+O\left(\frac{1}{n},\frac{n}{m}\right), \quad 0 \leqslant z \leqslant n^{-1}, \tag{2}$$

with $U(z) \approx 1$ for the core. Or, because $z \leqslant n^{-1} \ll 1$,

$$U(z) \approx 1-nz, \quad 0 \leqslant z \leqslant n^{-1}. \tag{3}$$

If we only consider axisymmetric disturbances of the cylindrical interface, because the paper by Preziosi *et al.* (1989) strongly suggests that these will always be the most unstable ones, the above shows that the most important instability of the interface can be described in a two-dimensional geometry. This leads to the simple geometry of two-dimensional Couette flow of two fluids of different viscosity, with the less viscous fluid bounded by a wall and the other fluid unbounded (or in a much thicker

layer than the first fluid; see figure 3). What we should note is that the possibility of capillary instability is ruled out by this choice. But as already noted in §2, this low-Reynolds-number instability was not observed.

In the following we will use a coordinate system that moves with the velocity of the fluids at the interface. The equations of motion, i.e. the Navier–Stokes equations, are non-dimensionalized with respect to d, the distance from the interface to the wall, and U, the velocity of the interface (and also of the whole core). This introduces the dimensionless coordinates x, y, the basic flow depicted in figure 3, and the following dimensionless parameters (see, for example, §3 of Yih 1967):

$$\left.\begin{aligned} R &= \rho_1 U d/\mu_1, \text{ the Reynolds number of the annulus,} \\ m &= \mu_2/\mu_1, \text{ the viscosity ratio} \\ r &= \rho_2/\rho_1, \text{ the density ratio,} \\ S &= T/(\rho_1 d U^2), \text{ the dimensionless surface tension parameter,} \\ \text{and} \quad F &= U^2/[(1-r)gd], \text{ the Froude number,} \end{aligned}\right\} \tag{4}$$

where ρ_i and μ_i are the density and the (dynamic) viscosity of fluid i, T is the surface tension, and g is the magnitude of the gravitational acceleration. As was done by Yih (1967), the Navier–Stokes equations, in stream function formulation, are linearized in the disturbance of the basic flow. We assume the disturbances to have an x- and t-dependence of the form $\exp[\mathrm{i}\alpha(x-ct)]$, where c is the dimensionless phase velocity of the disturbance in the x-direction. This velocity has to be determined in the course of the analysis. The growth rate of the disturbance is given by $\mathrm{Im}(\alpha c)$.

Then the y-dependent parts of the stream functions, $\phi_i(y)$, satisfy the well-known Orr–Sommerfeld equations (Orr 1907; Sommerfeld 1908):

$$\left(\frac{\mathrm{d}^2}{\mathrm{d}y^2}-\alpha^2\right)^2\phi_1(y) = \mathrm{i}\alpha R(y-c)\left(\frac{\mathrm{d}^2}{\mathrm{d}y^2}-\alpha^2\right)\phi_1(y) \quad \text{for} \quad -1 < y < 0, \tag{5}$$

$$\left(\frac{\mathrm{d}^2}{\mathrm{d}y^2}-\alpha^2\right)^2\phi_2(y) = -\frac{\mathrm{i}\alpha Rrc}{m}\left(\frac{d^2}{dy^2}-\alpha^2\right)\phi_2(y) \quad \text{for} \quad y > 0. \tag{6}$$

The no-penetration and the no-slip conditions at the boundary at $y = -1$ give

$$\phi_1(-1) = 0, \tag{7}$$

$$\phi_1'(-1) = 0 \tag{8}$$

where the prime denotes the derivative with respect to y. If the fluid is assumed to be unbounded, the solution has to be bounded as $y \to \infty$.

The conditions at the interface are the continuity of the velocity components and the balance of the stress components. Yih (1967) shows that these can be formulated as (see also Hooper & Boyd 1987)

$$\phi_1 = \phi_2 = \phi(0), \tag{9}$$

$$\phi_1' = \phi_2' + \frac{\phi(0)}{c}\frac{1-m}{m}, \tag{10}$$

$$\phi_1'' + \alpha^2\phi_1 = m(\phi_2'' + \alpha^2\phi_2), \tag{11}$$

$$\phi_1''' - 3\alpha^2\phi_1' = m(\phi_2''' - 3\alpha^2\phi_2') + \mathrm{i}\alpha R\left[(\alpha^2 S + F^{-1})\frac{\phi(0)}{c} + (r-1)\left(\frac{c\phi_2' + \phi(0)}{m}\right)\right], \tag{12}$$

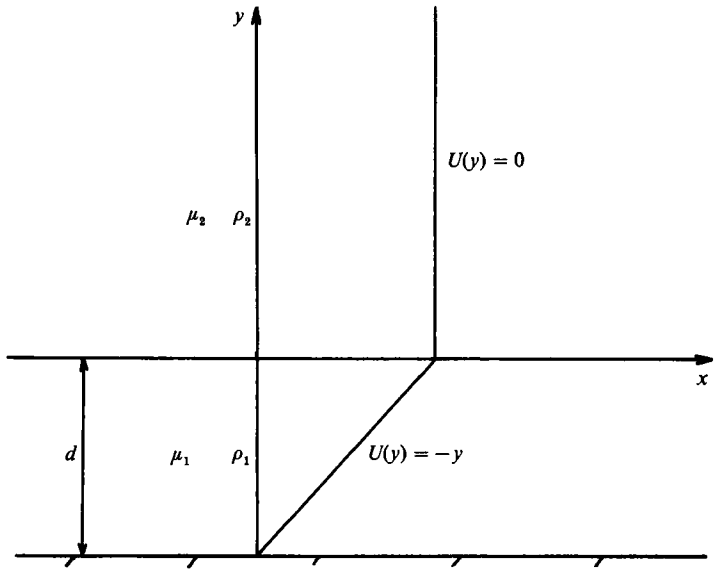

FIGURE 3. The configuration of the flow and the velocity profile $U(y)$. The less viscous fluid 1 (water) is bounded by the wall and fluid 2 (oil).

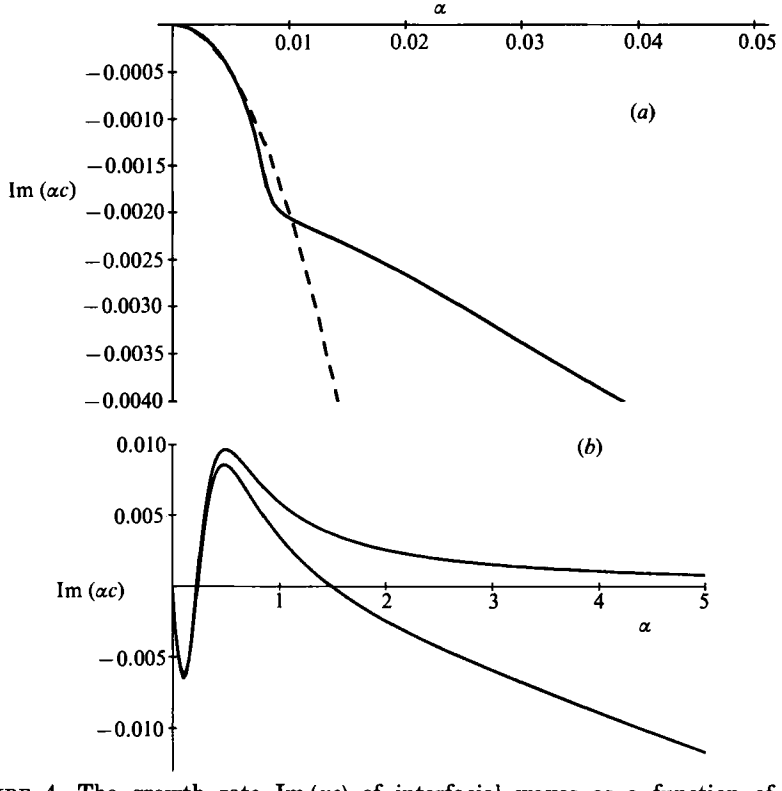

FIGURE 4. The growth rate $\mathrm{Im}(\alpha c)$ of interfacial waves as a function of the dimensionless wavenumber α, for $m = 10^4, R = 2500, S = 0.02, r = 0.97, F = 7.5 \times 10^{-4}$, and a ratio of the core radius to water layer thickness $n = 40$. In (a) the asymptotic result (13) for small α is shown (dashed line). In (b) the growth rate if surface tension is neglected is also shown, i.e. $S = 0$ (upper curve).

where we have used the equation for the continuity of the tangential velocity (10) to simplify the balance of the normal stress (12). Equations (5) and (6) will now be solved asymptotically, subject to the boundary and interface conditions (7)–(12). This gives the phase speed c and thus the growth rate $\mathrm{Im}(\alpha c)$. Furthermore, the asymptotic solution is checked numerically.

3.2. *Numerical solution*

Equations (5)–(12) are solved numerically by reducing them to an algebraic complex-valued generalized matrix eigenvalue problem, by using truncated expansions of the eigenfunctions in terms of Chebyshev polynomials (Orszag 1971), with eigenvalues c. We are then interested in the most unstable mode, corresponding to the eigenvalue for which the growth rate $\mathrm{Im}(\alpha c)$ is maximal. Since not all the boundary and interface conditions contain the eigenvalue c, infinite eigenvalues will arise. During the actual computation these infinite eigenvalues might interfere with the large but finite ones (Goussis & Pearlstein 1989). To remedy this the coefficients of the (two) highest-order Chebyshev polynomials are eliminated, giving rise to a slightly denser and smaller system that does not have the infinite eigenvalues.

For a given number of Chebyshev polynomials in the expansion all (complex) eigenvalues are computed, using the QZ algorithm as implemented in the Numerical Algorithm Group (NAG) library (Moler & Stewart 1973). The relevant matrices are balanced prior to the actual calculations (Osborne 1960). The main interest lies in the eigenvalue with the largest imaginary part.

The correctness of the numerical results was checked in several ways: the (numerical) results of Renardy (1985) were reproduced, as were the asymptotic results of Yih (1967) and Hooper & Boyd (1987). This could be done using 40 or less Chebyshev polynomials. A calculation of the growth rate of interfacial waves for characteristic values of the parameters m, R, and S is shown in figure 4. Also shown in figure 4 is the 'long' wavelength asymptotic result of Yih (1967), which for $m \gg n^2 \gg 1$ reduces to

$$\mathrm{Im}(\alpha c) \approx \frac{n^3(m^2 - 4mn^3 - 8n^6)}{15(m+4n^3)^3}\alpha^2 R. \tag{13}$$

Note that this means that the interface of the flow considered is stable to long-wavelength perturbations as long as $m < 2(1+\sqrt{3})n^3$ or $n > 0.57m^{\frac{1}{3}}$, a condition satisfied for most experiments. This means that no long waves (waves with wavelengths larger than $2\pi Rd$) will be observed if the thickness of the annulus is small enough.

The result in figure 4 was found to be almost independent of n,r, and F, indicating that the influence of the finite thickness of the second layer and of gravity are only minor. The high-wavenumber cutoff disappears if surface tension is neglected (see figure 4). Variations of the other parameters (within the limits relevant to the experiments) generally gives the same picture: stability of 'long' as well as 'short' waves ($\alpha \gg 1$), and a band of unstable wavenumbers, say $0.1 < \alpha < 2$, in between.

3.3. *Asymptotic solution*

We will now solve asymptotically the problem posed in §3.1: the Orr–Sommerfeld equations for the fluid in the annulus (5) and the fluid in the core (6), with boundary conditions (7), (8) and interfacial conditions (9)–(12). First some observations that are important for the analysis are repeated here. The waves in experiments satisfy $\alpha = O(1)$ and $R = O(10^3)$, so $\alpha R \gg 1$. The phase velocity of the waves c, in the frame

moving at the interfacial velocity of the fluids, is small. The ratio of the densities of the fluids $r \approx 1$. Finally, the ratio of the viscosities $m \geqslant O(\alpha R) \gg 1$.

3.3.1. *The stream function of the core*

First, the Orr–Sommerfeld equation (6) for the stream function related to the disturbance of the basic flow in the core, is solved. This can be done in terms of integrals of Airy functions (Hooper & Boyd 1987), but simpler solutions, leading to much simpler results, can be obtained by asymptotic approximation. Because $\alpha Rc/m \ll 1$, the right-hand side of (6) can be neglected with an error $O(\alpha Rc/m)$. This means that the flow is dominated by its viscosity, i.e. it is Stokes flow:

$$\left(\frac{\mathrm{d}^2}{\mathrm{d}y^2}-\alpha^2\right)^2 \phi_2(y) = 0, \tag{14}$$

with the solution

$$\phi_2(y) = (a_1 y + a_2)\,\mathrm{e}^{-\alpha y} + (a_3 y + a_4)\,\mathrm{e}^{\alpha y}. \tag{15}$$

The constants a_1 to a_4 are determined by the boundary and the interfacial conditions. Using boundary conditions similar to (7) and (8), a_3, a_4 can be expressed in terms of a_1, a_2 and it can be shown that the core can be approximated by an infinite layer if $2\alpha n \gg 1$, where n is the dimensionless thickness of the more viscous layer, i.e. the dimensionless core radius. Assuming that $2\alpha n \gg 1$, or equivalently that the fluid is infinite and the solution $\phi_2(y)$ is bounded, gives

$$\phi_2(y) = (a_1 y + a_2)\,\mathrm{e}^{-\alpha y}. \tag{16}$$

3.3.2. *The stream function of the annulus*

The solution of equation (5) for the stream function in the annulus is obtained by matched asymptotic expansions. Note that (5), like (6), can also be solved exactly; however, these exact solutions are complicated to handle.

From (5) it is clear, because $\alpha R \gg 1$, that the left-hand side of that equation can be neglected correct to $O(\alpha R)^{-1}$. The terms on the left-hand side of the equation represent the viscous terms in the Navier–Stokes equations. So, in contrast to the disturbance in the core, the disturbance in the annulus appears to be dominated by the 'connective' terms of the Navier–Stokes equations. However, this approximation is only justified if the derivatives with respect to y occurring in (5) are not too large. This is correct outside the (viscous) boundary layers at the wall and at the interface. In the boundary layers a different approximation is used, in which the fourth-order derivative is balanced by the largest (non-viscous) term on the right-hand side of the Orr–Sommerfeld equation. The solution of that equation is then matched to the solution in the main part of the fluid.

Another complication is associated with the position of the critical layer, at $y-c = 0$, where the phase velocity of the disturbance becomes equal to the velocity of the basic flow. If the critical layer is outside the boundary layers, it can be shown (see, for example, Drazin & Reid 1981) that the solution has the same form inside the critical layer as outside it if the basic velocity profile has zero curvature, as in our problem. However, if the critical layer is inside a boundary layer, the standard way of dealing with a viscous boundary layer becomes invalid. Because it was observed in the experiments that the phase speed of the waves is almost equal to the velocity of the core and the velocity of the fluid of the annulus at the interface, we indeed expect the critical layer to be in the boundary layer at the interface. For the

boundary layer at the interface we will therefore use a different scaling than the one that is used for the boundary layer at the wall.

Outside the boundary layers the Orr–Sommerfeld equation (5) can be approximated ($\alpha \gg 1$) by

$$\left(\frac{\mathrm{d}^2}{\mathrm{d}y^2}-\alpha^2\right)\phi_1^{\mathrm{o}}(y) = 0, \tag{17}$$

with the outer $\phi_1^{\mathrm{o}}(y)$ solution given by

$$\phi_1^{\mathrm{o}}(y) = b_1\,\mathrm{e}^{\alpha y}+b_2\,\mathrm{e}^{-\alpha y}. \tag{18}$$

To determine a solution $\phi_1^{\mathrm{w}}(y)$ near the wall $y=-1$, the coordinate y is scaled so that the fourth-order derivative is of the same magnitude as the right-hand side (non-viscous terms) of (5). This equation is then solved, correct to the lowest order in the scaling parameter, and matched with the outer solution (18). Following Hooper & Boyd (1987, equations (3.4) to (3.11)) we find:

$$\phi_1^{\mathrm{w}}(y) = d_1\left\{\sinh\left[\alpha(y+1)\right]-\frac{\epsilon_{\mathrm{w}}\alpha}{p}\cosh\left[\alpha(y+1)\right]+\frac{\epsilon_{\mathrm{w}}\alpha}{p}\mathrm{e}^{-p(y+1)/\epsilon_{\mathrm{w}}}\right\}, \tag{19}$$

$$\begin{aligned}\phi_1^{\mathrm{o}}(y) &= d_1\left\{\sinh\left[\alpha(y+1)\right]-\frac{\epsilon_{\mathrm{w}}\alpha}{p}\cosh\left[\alpha(y)+1)\right]\right\}\\ &\approx d_1\sinh\left[\alpha(y+1)\right],\end{aligned} \tag{20}$$

where $\epsilon_{\mathrm{w}} = (\alpha R)^{-\frac{1}{2}} \ll 1$ and $p = \exp\left(-\frac{1}{4}\mathrm{i}\pi\right)$.

Because we observed that waves have almost the same velocity as the fluids at the interface, we assume that $c \ll 1$ (c is the phase velocity in the frame moving at the interfacial speed). Therefore, in the boundary layer near the interface, $|y-c| \ll 1$, in contrast to $|y-c| \approx 1$ in the boundary layer near the wall, and a different scaling from the one near the wall is needed near the interface in order to balance the fourth-order derivative with the leading terms on the right-hand side of (5):

$$z = y/\epsilon, \tag{21}$$

where a suitable choice of ϵ is found to be

$$\epsilon = (\alpha R)^{-\frac{1}{3}}. \tag{22}$$

The leading-order terms of (5) then give

$$\left[\frac{\mathrm{d}^2}{\mathrm{d}z^2}-\mathrm{i}(z-c/\epsilon)\right]\omega_1(z) = 0, \tag{23}$$

$$\omega_1(z) := \frac{\mathrm{d}^2\phi_1^{\mathrm{i}}}{\mathrm{d}z^2}, \tag{24}$$

where $\phi_1^{\mathrm{i}}(z)$ is the solution for ϕ_1 near the interface. The scaling (22) is chosen in such a way that both z and c/ϵ are $O(1)$, and this should be checked *a posteriori* (see (36)). Equation (23) can be solved in terms of Airy functions:

$$\omega_1(z) = e_1\,\mathrm{Ai}\left[\mathrm{e}^{5\mathrm{i}\pi/6}(z-c/\epsilon)\right]+f_1\,\mathrm{Ai}\,\mathrm{e}^{\mathrm{i}\pi/6}(z-c/\epsilon)], \tag{25}$$

where e_1, f_1 are constants. From this, (24) can be solved for ϕ_1^{i} by integrating

twice. If ϕ_1^1 is matched with ϕ_1^0 we find that ϕ_1^1, and therefore $\omega_1(z)$, should be finite as $z \to -\infty$. This gives $f_1 = 0$. Solving for ϕ_1^1 then gives

$$\phi_1^1(z) = \int_{-\infty}^{z} \mathrm{d}\tilde{z} \int_{-\infty}^{\tilde{z}} \omega_1(\tilde{\tilde{z}})\, \mathrm{d}\tilde{\tilde{z}} + e_2 z + e_3, \tag{26}$$

where e_2, e_3 are constants. The lower boundaries of the integrals have been chosen such that matching is simple. Matching the solution near the interface (26) with the outer solution (20) is done by taking $|y| \ll 1$, i.e. $|\epsilon z| \ll 1$, and $|y/\epsilon| \gg 1$, i.e. $\|z\| \gg 1$. This gives

$$e_3 = \mathrm{d}_1 \sinh(\alpha), \tag{27}$$

$$e_2 = 0, \tag{28}$$

which, together with (25) and (26), yields

$$\phi_1^1(y) = (\alpha R)^{\frac{1}{3}} e_1 \int_{-\infty}^{y} \mathrm{d}\tilde{y} \int_{-\infty}^{\tilde{y}} \mathrm{Ai}\left[\mathrm{e}^{5\mathrm{i}\pi/6}(\alpha R)^{\frac{1}{3}}(\tilde{\tilde{y}} - c)\right] \mathrm{d}\tilde{\tilde{y}} + d_1 \sinh(\alpha). \tag{29}$$

3.3.3. *The interfacial conditions*

In the foregoing subsections we have determined the solutions of the Orr–Sommerfeld equations for the stream functions of the flow in the core (§3.3.1) and the annulus (§3.3.2). These solutions should satisfy the conditions for continuity of velocity and stress at the interface given by (9)–(12). These (four) interfacial conditions fix the four constants a_1, a_2, d_1, e_1, occurring in the solutions for the stream functions (16), (19), (20), and (29), up to a common constant, and they determine the value of the phase speed c.

From the continuity of the normal velocity at the interface (9) and the stream functions on both sides of the interface (16) and (29) we find

$$a_2 = d_1 \sinh(\alpha) + (\alpha R)^{\frac{1}{3}} e_1 \int_{-\infty}^{0} \mathrm{d}\tilde{y} \int_{-\infty}^{\tilde{y}} \mathrm{Ai}\left[\mathrm{e}^{5\mathrm{i}\pi/6}(\alpha R)^{\frac{1}{3}}(\tilde{\tilde{y}} - c)\right] \mathrm{d}\tilde{\tilde{y}}. \tag{30}$$

From (10) (continuity of the tangential velocity) the leading terms, i.e. the term of $O(\alpha R)^{\frac{1}{3}}$ on the left-hand side and the term proportional to $c^{-1} = O(\alpha R)^{\frac{1}{3}}$ on the right-hand side, give

$$e_1 = -\frac{a_2}{cJ(\alpha R)^{\frac{1}{3}}}, \tag{31}$$

where

$$J = \int_{-\infty}^{0} \mathrm{Ai}\left[\mathrm{e}^{5\mathrm{i}\pi/6}(\alpha R)^{\frac{1}{3}}(\tilde{y} - c)\right] \mathrm{d}\tilde{y}. \tag{32}$$

The tangential stress conditions (11) gives, using $m \geqslant O(\alpha R)^{\frac{2}{3}}$,

$$a_1 = \alpha a_2. \tag{33}$$

Finally, we consider the equation resulting from the balance of the normal stress. The leading terms are $O(m)$ and $O(\alpha R)^{\frac{2}{3}}$:

$$(\alpha R)^{\frac{1}{3}} e_1 \mathrm{Ai}' = (2m\alpha + \mathrm{i}\alpha RS/c)\, \alpha^2 a_2, \tag{34}$$

$$\mathrm{Ai}' = \left\{\frac{\mathrm{d}}{\mathrm{d}y} \mathrm{Ai}\left[\mathrm{e}^{5\mathrm{i}\pi/6}(\alpha R)^{\frac{1}{3}}(y - c)\right]\right\}\Big|_{y=0}, \tag{35}$$

where we have used $F^{-1} \ll \alpha^2 S$, and assumed that, $\alpha RS/c \leqslant O(m)$ or $S \leqslant O[m(\alpha R)^{-\frac{4}{3}}]$.

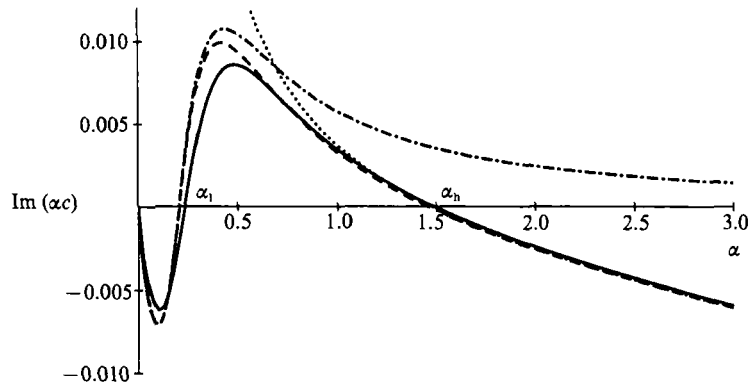

FIGURE 5. The growth rate as a function of the wavenumber for $R = 2500$, $S = 0.02$, $m = 10^4$. The solid line is part of the curve depicted in figure 4. The dashed line is calculated from (36), together with (37) and (38). This calculation was done using only the function 'Solve' of the *Mathematica* software package. The dashed-dotted line is for zero surface tension ($S = 0$). The dotted line is given by the asymptotic expression (39). Also shown are the wavenumbers α_l numbers and α_h at which the growth rate is zero.

3.3.4. *The results of the analysis*

Combining (31) and (34) finally gives

$$\alpha c = -\frac{1}{2m}[\mathrm{i}\alpha RS + \mathrm{Ai}'/(\alpha^2 J)], \tag{36}$$

where Ai′ and J are given by (35) and (32), respectively. This equation also shows that c is indeed $O(\alpha R)^{-\frac{1}{3}}$. From this expression the growth rate can be calculated. Furthermore, the stream functions in both the annulus and the core, that is (16), (19), (20), and (29), are now given by (36), together with (30), (31), and (33). As we can see from (36), the growth rate is roughly inversely proportional to the ratio of the viscosities: the more viscous the core or the less viscous the annulus, the more slowly disturbances will grow. It can further be seen that the surface tension contributes negatively to the growth rate and is more important for shorter waves (larger α).

The problem in calculating the growth rate $\mathrm{Im}(\alpha c)$ from (36) is that J and Ai′ depend on c, so that the growth rate is in fact only implicitly given by (36). This problem can be solved by approximating both J and Ai′ by the first terms of their Taylor expansions round $c = 0$:

$$\begin{aligned} J &\approx \int_{-\infty}^{0} \mathrm{Ai}\,[\mathrm{e}^{5\mathrm{i}\pi/6}(\alpha R)^{\frac{1}{3}}\tilde{y}]\,\mathrm{d}\tilde{y} - c\,\mathrm{Ai}\,(0) \\ &= \tfrac{1}{3}(\alpha R)^{-\frac{1}{3}}\mathrm{e}^{\mathrm{i}\pi/6} - 0.3550c, \end{aligned} \tag{37}$$

$$\begin{aligned} \mathrm{Ai}' &\approx (\alpha R)^{\frac{1}{3}}\mathrm{e}^{5\mathrm{i}\pi/6}[\mathrm{Ai}'(0) + \mathrm{Ai}''(0)\,(\alpha R)^{\frac{1}{3}}\mathrm{e}^{-\mathrm{i}\pi/6}c + \tfrac{1}{2}\mathrm{Ai}'''(0)\,(\alpha R)^{\frac{2}{3}}\mathrm{e}^{-\mathrm{i}\pi/3}c^2] \\ &= (\alpha R)^{\frac{1}{3}}\mathrm{e}^{-\mathrm{i}\pi/6}[0.2588 - 0.1775(\alpha R)^{\frac{2}{3}}\mathrm{e}^{-\mathrm{i}\pi/3}c^2], \end{aligned} \tag{38}$$

where one has to be careful with the definition of the domain of the Airy functions and thus with the value (and sign) of Ai(0), Ai′(0), Ai″(0), and Ai‴(0). Using these two approximations (36) is just a (complex) quadratic equation in c, from which the growth rate can be calculated very easily, using a standard software package such as, for example, *Mathematica*. The agreement between this approximation and the numerical solution of §3.1 is quite good (figure 5), and becomes better if higher-order terms in (37), (38) are taken into account. Also shown in figure 5 is the result if

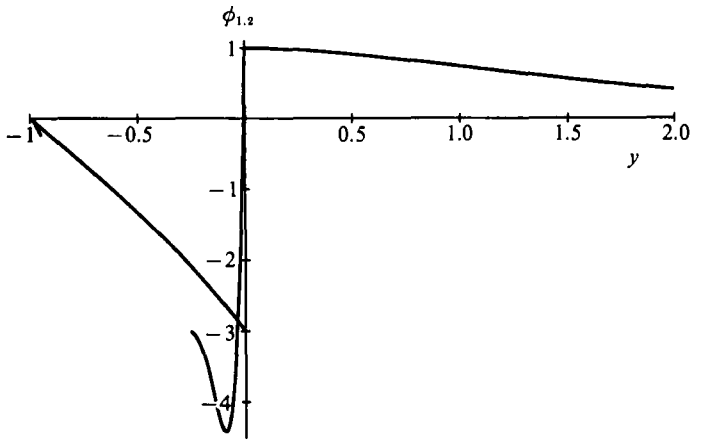

FIGURE 6. The stream functions for $\alpha = 1$, $a_2 = 1$, and $R = 2500$, $S = 0.02$, $m = 10^4$. Note that the part of stream function that is valid near the wall ($y = -1$) can be distinguished from the outer solution only very near the wall. This should be expected because the thickness of the boundary layer near the wall is of order $(\alpha R)^{-\frac{1}{3}} = 0.02$. The stream function near the interface, however, differs substantially from the outer solution. It is valid in the boundary layer near the interface which is approximately $(\alpha R)^{-\frac{1}{3}} \approx 0.1$ thick. These functions have been calculated using (16), (19), (20), (29), (30), (31), (33), (36), (37), and (38). The values obtained, and used, for c and J were $c = (-3.901 + 3.285\mathrm{i})\ 10^{-3}$, $J = (2.265 + 1.111\mathrm{i})\ 10^{-2}$.

surface tension is neglected ($S = 0$). As expected, in that case the growth rate is positive for large wavenumbers, and there is no cutoff. As an example, in figure 6 the stream function is given for the same parameters used in figure 5.

For larger wavenumbers only the first term in (37) and (38) seems to be important (see also Hooper & Boyd 1983), so that the growth rate is given by (see also figure 5):

$$\mathrm{Im}\,(\alpha c) = \frac{1}{2m}[-\alpha RS + 0.6724(R/\alpha^2)^{\frac{2}{3}}]. \tag{39}$$

Thus an approximation for the maximum wavenumber with a positive growth rate, i.e. the 'high-wavenumber cutoff' α_h, can be found to be (figure 5, figure 7)

$$\alpha_h = 0.844(RS^3)^{-\frac{1}{7}}. \tag{40}$$

A more rigorous way to obtain this expression is given in the Appendix. Note that (in this approximation) it is independent of the ratio of the viscosities m of the two fluids and only weakly dependent on the Reynolds number. It should be noted that a better approximation can be obtained from (36).

For smaller wavenumbers surface tension will be less important. Neglecting surface tension, and using (36) together with (37) and (38), the lower wavenumber α_l where the growth rate is zero (figure 5, figure 7) can be approximated by

$$\alpha_l = 0.409(R/m)^{\frac{1}{3}}. \tag{41}$$

As is shown in the Appendix, this approximation is correct if $S \ll O(m^{\frac{7}{3}}/R^{\frac{8}{3}})$, so that it is better for smaller S, larger m, and smaller R. The Appendix also shows that the curve of neutral stability is determined not by the four independent parameters α, R, m, S, but by the two parameters $m\alpha^2/R$; cf. (41); and $\alpha^2(\alpha R)^{\frac{1}{3}}S$; cf. (40). The curve of neutral stability in that parameter space is shown in figure 8.

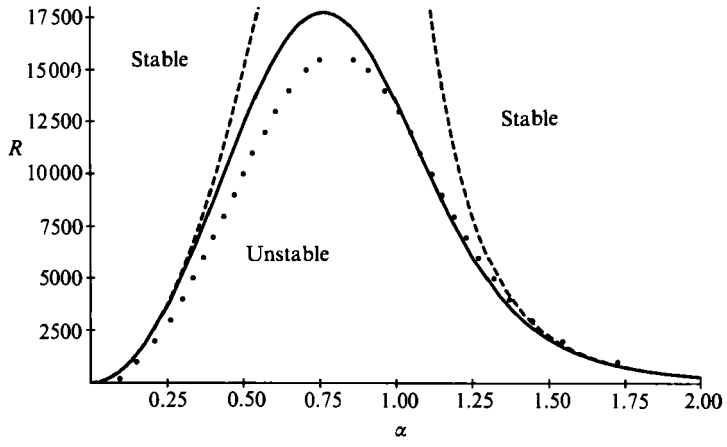

FIGURE 7. Lines of neutral stability (zero growth rate) in an (α, R) plot. The solid lines are calculated using the (A 6) in the Appendix, which was derived from (36), (37), and (38). The dashed lines are the approximations ($m = 10^4$, $S = 0.02$) given by (40) and (41), respectively. The dots are determined numerically for $m = 10^4$, $S = 0.02$, $r = 0.97$, $F = 7.5 \times 10^{-4}$.

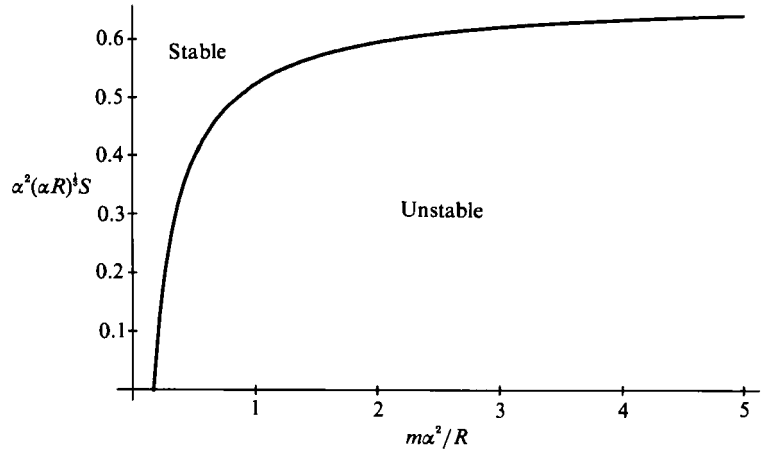

FIGURE 8. The curve of neutral stability calculated from (A 6) in the Appendix. The x-axis is the parameter $m\alpha^2/R$, the y-axis the parameter $a^2(\alpha R)^{\frac{1}{3}}S$. The values of these two parameters determine whether a disturbance with wavelength α grows.

At the end of this section we note that (36) looks very much like (28) of Hooper & Boyd (1983), although it is used in a different context and other approximations have been used. This is rather surprising because Hooper & Boyd considered a geometry of two infinite fluids, while we considered only one infinite fluid, the other being finite. This means that the instability is determined predominantly by the viscous boundary layer near the interface. The influence of the wall and the boundary layer near it seems to be negligible.

4. Discussion and conclusions

The theory presented in the previous section agrees quantitatively very well with the general results of the experiments given in §2. For lubricating CAF with a thin annulus, a very large viscosity ratio of the fluids, a large Reynolds number for the

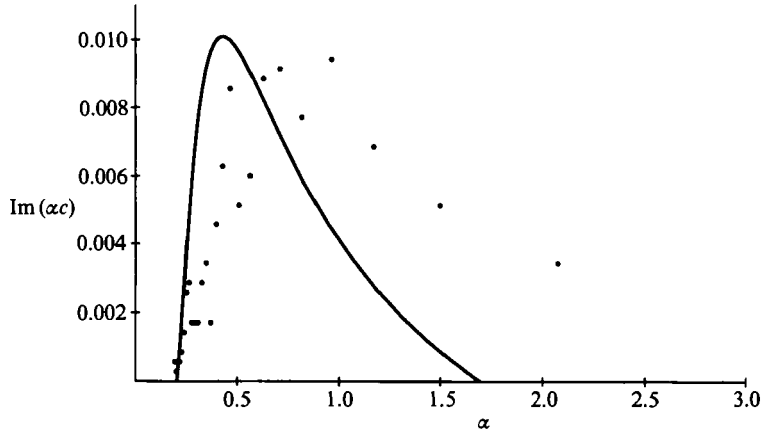

FIGURE 9. Calculated growth rate and measured wavelength distribution for a characteristic experiment in an 8 in. pipe. The dots represent the measured wavelength distribution for an experiment in an 8 in. pipe, with a viscous crude oil (viscosity $\approx$ 10 Pa s) as the fluid in the core and water (viscosity $\approx 9.5 \times 10^{-4}$) as the lubricating fluid in the annulus. The relevant quantities are the mean water layer thickness $d = 4.3$ mm and core velocity $U = 0.58\ \mathrm{m\ s^{-1}}$, giving a Reynolds number $R = 2600$. The surface tension was $0.02\ \mathrm{N\ m^{-1}}$, giving a surface tension parameter $S = 0.014$. The solid line is the (positive part of the) growth rate, for $m = 10^4$, $R = 2600$, $S = 0.014$. The wavenumbers α_1 and α_h are the minimum and maximum wavenumbers for which the growth rate is positive, respectively.

fluid in the annulus, and wave speeds close to the speed of the core, the theory correctly predicts that waves will exist with wavelengths of approximately 1–10 times the thickness of the annulus. The band of wavelengths will be broader for larger viscosity ratios, and smaller Reynolds number or surface tension. In this section we will make a quantitative comparison between the experiments and the theory and provide an explanation for the discrepancies. We will use mainly the results from the 2 in. pipe, because more data are available there.

One data set for the 8 in. pipe is given in figure 9, covering that part of the growth rate *vs.* wavenumber curve for which the growth rate is positive. The idea that the measured wavelength distribution is in some way proportional to the growth rate can only be defended with 'hand-waving' arguments, and as kind of extension of the idea in hydrodynamics that the mode with the largest growth rate will be the dominant one. Thus, assume that the wavelength distribution has its maximum at the wavenumber where the growth rate is maximal, and assume that waves corresponding to wavenumbers with negative growth rates will not be observed. It then seems reasonable to compare the curve for the growth rate as a function of the wavenumber and the wavelength distribution. For the experiment depicted in figure 9 we see a very good agreement between the smallest wavenumber observed, and the smallest wavenumber with a positive rate α_1, as predicted by the theory. The largest observed wavenumber α_h and the wavenumber at which the experimental wavelength distribution has its maximum are, however, considerably larger than predicted by the theory (about a factor of 2). This may be explained only partly by a surface tension that is reduced, e.g. by fouling, so that the high-wavenumber cutoff becomes larger. Another explanation concerns nonlinear effects, which we have neglected. These effects will be important because the amplitudes of the observed waves are large. Examples are the disturbance of the (linear) basic flow, and the generation of higher harmonics by nonlinear interaction. We also should not forget

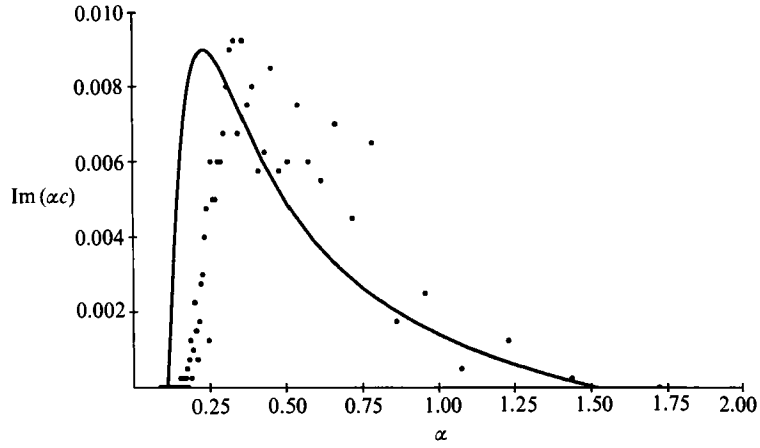

FIGURE 10. Calculated growth rate and measured wavelength distribution for a characteristic experiment in a 2 in. pipe. The dots represent the measured wavelength distribution for an experiment in a 2 in pipe, with a viscous fuel oil (viscosity $\approx$ 21 Pa s) as the fluid in the core and water (viscosity $\approx 1.3 \times 10^{-3}$ Pa s) as the lubricating fluid in the annulus. The mean water layer thickness $d = 1.4$ mm and the core velocity $U = 1.1$ m s^{-1}, giving a Reynolds number $Re = 1200$. The surface tension was 0.04 N m^{-1}, giving a surface tension parameter $S = 0.024$. The solid line is the (positive part of the) growth rate, for $m = 1.6 \times 10^4$, $R = 1200$, $S = 0.024$.

that experimental errors in the wavenumber, the Reynolds number, and the surface tension parameter may be of the order of 10–20 %. This error is mainly caused by the uncertainty in the measured core speed, which is used to calculate the quantities mentioned above. Important parameter values for this experiment are: core/annulus thickness ratio $\approx$ 25, viscosity ratio 10^4, Reynolds number 2600, and surface tension parameter $S = 0.014$, so that the assumptions made in the analysis are indeed correct.

A typical dimensionless growth rate for these experiments is 0.01. With a velocity of 1 ms^{-1} and an annulus thickness of 4 mm this gives a dimensional growth rate of 2.5 s^{-1}, which means that the amplitude of a disturbance grows by a factor e in $\frac{1}{2.5}$ of a second. This implies that waves will form almost instantaneously on the surface of the core, which is necessary in order for the flow not to break down due to the core touching the upper pipe wall (Oliemans & Ooms 1986).

Figure 10 shows equivalent data for the 2 in. pipe. In this example we see a less good agreement between the smallest wavenumber observed and α_l, but a very good agreement between the largest wavenumber observed and α_h (although it should be noted that the wavelength corresponding to the data point at $\alpha \approx 1.7$ is quite close to the lower limit of our measuring system. The other points are not, however, and the cutoff was also observed in experiments where it was less close to this limit.) The wavenumber at which the experimental wavelength distribution has its maximum corresponds well to the wavenumber for which the calculated growth rate is maximal. This is the case in most of the experiments in the 2 in. pipe.

From the large number of other experiments that were done, only a few representative data are presented here. The shape of the measured wavenumber distribution in general looks like the one in figure 10, with the location of the maximum of the wavelength distribution approximately coinciding with the location of the maximum growth rate. We therefore concentrate on the smallest and the largest wavenumbers, and compare these with the theoretical predictions. As can be seen from table 2, the smallest and largest observed wavenumbers for the experiments

			α_l		α_h	
m	R	S	Theory	Experiment	Theory	Experiment
3600	720	0.075	0.19	0.21	0.97	1.48
3600	1530	0.018	0.27	0.23	1.62	1.56
4000	2930	0.0049	0.35	0.18	2.62	1.59
17700	310	0.17	0.061	0.13	0.76	0.72
16200	1570	0.017	0.13	0.17	1.68	1.41
16200	3200	0.0060	0.18	0.24	2.38	2.32

TABLE 2. Six representative experiments in the 2 in. pipe, with theoretical and experimental values for low- and high-wavenumber cutoffs for positive growth rates.

with the smaller viscosity ratio seem to be more or less independent of the parameters R and S, contradicting the theory. This is not caused by the approximations made in the analysis, because comparison with numerical results shows very good agreement. If this disagreement were caused by the experimental method we would expect about the same picture for the other experiments. However, the experiments at a higher ratio of the viscosities do agree much better with the calculations, so that this possibility appears not to apply. A possible explanation, that cannot be checked, is that it is a nonlinear effect, examples of which have already been mentioned above, which is more important at lower viscosity ratio. Also the onset of turbulence as observed in the water layer is possibly of some importance. Finally, for the 2 in. pipe for the larger wavenumbers (smaller wavelengths), the lower limit (5 mm) of the wavelength measurement is reached, so that for these wavelengths the inaccuracy can be large.

The inclusion of (weakly) nonlinear effects in the theory of the interfacial stability of CAF with large viscosity ratios, displaying, for example, the important effect of nonlinear saturation of the growth of the waves, would seem to be the next step in the theoretical development.

Appendix. Neutral curves

Equation (36) can be written

$$2m\alpha^3 cJ + \mathrm{Ai}' + \mathrm{i}\alpha^3 RSJ = 0. \tag{A 1}$$

Assuming that the imaginary part of c is zero and introducing $\tilde{c} = (\alpha R)^{\frac{1}{3}}c$ gives, together with (37) and (38),

$$\tilde{c}^2(-0.71m\alpha^3) + \tilde{c}(\tfrac{1}{3}\sqrt{3}m\alpha^3) + (0.1294\sqrt{3}\alpha R - \tfrac{1}{6}(\alpha R)^{\frac{4}{3}}\alpha^2 S) = 0, \tag{A 2}$$

$$\tilde{c}^2(0.1775\alpha R) + \tilde{c}(\tfrac{1}{3}m\alpha^3 - 0.3550(\alpha R)^{\frac{4}{3}}\alpha^2 S) + (-0.1294\alpha R + \tfrac{1}{6}\sqrt{3}(aR)^{\frac{4}{3}}\alpha^2 S) = 0. \tag{A 3}$$

Elimination of $\tilde{c}^2$ from one of these two equations gives

$$\tilde{c}[1.878x^2 + (0.8132 - 2y)x] = (0.7290 - 1.266y)x + (0.2347y - 0.3157), \tag{A 4}$$

$$\tilde{c}^2 + \tilde{c}(1.878x - 2y) + (-0.7290 + 1.626y) = 0, \tag{A 5}$$

where $x = m\alpha^2/R, y = \alpha^2(\alpha R)^{\frac{1}{3}}S$. Eliminating $\tilde{c}$ gives

$$\begin{aligned} x^3(2.227 - 3.311y) + x^2(0.4328 - 2.620y + 1.764y^2) \\ + x(0.4603 - 1.882y + 2.408y^2 - 0.9388y^3) \\ + (-0.09967 + 0.1482y - 0.05508y^2) = 0. \end{aligned} \tag{A 6}$$

Neglecting surface tension, that is, assuming that $y \ll x$, yields

$$x^3 + 0.1943x^2 + 0.2067x - 0.04476 = 0, \tag{A 7}$$

with the (real) solution $x = 0.1675$, so that (cf. (41))

$$\alpha_1^2 = 0.1675R/m. \tag{A 8}$$

This approximation is justified if $y \ll x$, i.e.

$$S \ll m/R(\alpha R)^{-\frac{1}{3}} = O(m^{\frac{7}{6}}/R^{\frac{3}{2}}). \tag{A 9}$$

For larger wavenumbers, that is larger x (and a small enough surface tension parameter S), the first term of (A 6) is the most important one, so that $y \approx 0.6726$, i.e.

$$\alpha^{\frac{7}{3}} R^{\frac{1}{3}} S = 0.6726, \tag{A 10}$$

which is equivalent to (40).

REFERENCES

Charles, M. E., Govier, G. W. & Hodgson, G. W. 1961. The horizontal pipeline flow of equal density oil–water mixtures. *Can. J. Chem. Engng* **39**, 17–36.

Drazin, P. G. & Reid, W. H. 1981. *Hydrodynamic Stability*. Cambridge University Press.

Frenkel, A. L., Babchin, A. J., Levich, B. G., Shlang, T. & Sivashinsky, G. I. 1987 Annular flows can keep unstable films from breakup: Nonlinear saturation of capillary instability. *J. Colloid. Interface Sci. J. Colloid. Interface.* **115**, 225–233.

Goussis, D. A. & Pearlstein, A. J. 1989 Removal of infinite eigenvalues in the generalized matrix eigenvalue problem. *J. Comput. Phys.* **84**, 242–246.

Hickox, C. E. 1971 Instability due to viscosity and density stratification in axisymmetric pipe flow. *Phys. Fluids* **14**, 251–262.

Hooper, A. P. 1985 Long-wave instability at the interface between two viscous fluids: Thin layer effects. *Phys. Fluids* **28**, 1613–1618.

Hooper, A. P. & Boyd, W. G. C. 1983 Shear-flow instability at the interface between two viscous fluids. *J. Fluid Mech.* **128**, 507–528.

Hooper, A. P. & Boyd, W. G. C. 1987 Shear-flow instability due to a wall and a viscosity discontinuity at the interface. *J. Fluid Mech.* **178**, 201–225.

Hooper, A. P. & Grimshaw, R. 1985 Nonlinear instability at the interface between two viscous fluids. *Phys. Fluids* **28**, 37–45.

Hu. H. H., Lundgren, T. S. & Joseph, D. D. 1990 Stability of core–annular flow with a small viscosity ratio. *Phys. Fluids* A **2**, 1945–1954.

Joseph, D. D., Renardy, M. & Renardy, Y. 1984 Instability of the flow of two immiscible liquids with different viscosities in a pipe. *J. Fluid Mech.* **141**, 309–317.

Moler, C. B. & Stewart, G. W. 1973 An algorithm for generalized eigenvalue problems. *SIAM J. Numer. Anal.* **10**, 241–255.

Oliemans, R. V. A. 1986 The lubricating-film model for core-annular flow. Thesis, Delft University of Technology, Netherlands, 146 p.

Oliemans, R. V. A. & Ooms, G. 1986 Core-annular flow of oil and water through a pipeline. In *Multiphase Science and Technology*, Vol. 2 (ed G. F. Hewitt, J. M. Delhaye & N. Zuber). Hemisphere.

Ooms, G., Segal, A., Van der Wees, A. J., Meerhoff, R. & Oliemans, R. V. A. 1984 A theoretical model for core-annular flow of a very viscous oil core and a water annulus through a horizontal pipe. *Intl J. Multiphase Flow* **1**, 41–60.

Orr, W. M. F. 1907 The stability or instability of the steady motion of a perfect liquid and of a viscous fluid. *Proc. R. Irish Acad.* A**27**, 9–68; 69–138.

Orszag, S. A. 1971 Accurate solution of the Orr–Sommerfeld stability equation. *J. Fluid Mech.* **50**, 689–703.

Osborne, E. E. 1960 On pre-conditioning of matrices. *J. Assoc. Comput. Mach.* **7**, 338–345.

PAPAGEORGIOU, D. T., MALDARELLI, C. & RUMSCHITZKI, D. S. 1990 Nonlinear interfacial stability of core–annular film flows. *Phys. Fluids* A **2**, 340–352.

PREZIOSI, L., CHEN, K. & JOSEPH, D. D. 1989 Lubricated pipelining: stability of core–annular flow. *J. Fluid Mech.* **201**, 323–356.

RENARDY, Y. 1985 Instability at the interface between two sharing fluids in a channel. *Phys. Fluids* **28**, 3441–3443.

SHLANG, T., SIVASHINSKY, G. I., BABCHIN, A. J. & FRENKEL, A. L. 1985 Irregular wavy flow due to viscous stratification. *J. Phys. Paris* **46**, 863–866.

SOMMERFELD, A. 1908 Ein betrag zur hydrodynamische erklaerung der turbulenten Fluessigkeitsbewegungen. In *Proc. 4th Intl Congress of Mathematicians, Rome*, vol. 3, pp. 116–124.

THAN, P. T., ROSSO, F. & JOSEPH, D. D. 1987 Instability of Poiseuille flow of two immiscible liquids with different viscosities in a channel. *Intl J. Engng. Sci.* **25**, 189–204.

WU, H. L., DUIJVESTIJN, P. E. M., PATERNO, J. & GUEVERA E. 1986 Core-annular flow: A solution to pipeline transportation of heavy crude oils. *Rev. Tec. Intevep Venezuela* **6**, 17–22.

YIANTSIOS, G. Y. & HIGGINS, B. G. 1988 Linear stability of plane Poiseuille flow of two superposed fluids. *Phys. Fluids* **31**, 3225–3238.

YIH, C.-S. 1967 Instability due to viscosity stratification. *J. Fluid Mech.* **27**, 337–352.